POLITECNICO DI TORINO
Repository ISTITUZIONALE

Water electrolysis

Original
Water electrolysis / Shih, Arthur J.; Monteiro, Mariana C. O.; Dattila, Federico; Pavesi, Davide; Philips, Matthew; da Silva, Alisson H. M.; Vos, Rafaël E.; Ojha, Kasinath; Park, Sunghak; van der Heijden, Onno; Marcandalli, Giulia; Goyal, Akansha; Villalba, Matias; Chen, Xiaoting; Kasun Kalhara Gunasooriya, G. T.; Mccrum, Ian; Mom, Rik; López, Núria; Koper, Marc T. M.. - In: NATURE REVIEWS METHODS PRIMERS. - ISSN 2662-8449. - 2:1(2022). [10.1038/s43586-022-00164-0]

Availability:
This version is available at: 11583/2981919 since: 2023-09-11T09:25:45Z

Publisher:
Springer Nature

Published
DOI:10.1038/s43586-022-00164-0

Terms of use:

This article is made available under terms and conditions as specified in the corresponding bibliographic description in the repository

Publisher copyright
GENERICO -- per es. Nature : semplice rinvio dal preprint/submitted, o postprint/AAM [ex default]

The original publication is available at https://www.nature.com/articles/s43586-022-00164-0 / http://dx.doi.org/10.1038/s43586-022-00164-0.

(Article begins on next page)

07 August 2024

Supplementary Information

Water Electrolysis

Arthur J. Shih[1,6,#,*], Mariana C. O. Monteiro[1,7,#], Federico Dattila[2,8], Davide Pavesi[1], Matthew Philips[1], Alisson H. M. da Silva[1], Rafaël E. Vos[1], Kasinath Ojha[1,9], Sunghak Park[1], Onno van der Heijden[1], Giulia Marcandalli[1], Akansha Goyal[1], Matias Villalba[1], Xiaoting Chen[1], G. T. Kasun Kalhara Gunasooriya[4,5,*], Ian McCrum[3,*], Rik Mom[1,*], Núria López[2,*], Marc T.M. Koper[1,*]

[1] Leiden Institute of Chemistry, Leiden University, 2300 RA Leiden, The Netherlands
[2] Institute of Chemical Research of Catalonia (ICIQ), The Barcelona Institute of Science and Technology (BIST), 43007 Tarragona, Spain
[3] Department of Chemical and Biomolecular Engineering, Clarkson University, Potsdam, New York 13699, USA
[4] Department of Physics, Technical University of Denmark, 2800, Kongens Lyngby, Denmark
[5] School of Chemical, Biological, and Materials Engineering, University of Oklahoma, Norman, OK 73019, USA
[6] Current address: Department of Materials Science and Engineering, Northwestern University, Evanston, Illinois 60208, USA
[7] Current address: Fritz Haber Institute of the Max Planck Society, Faradayweg 4-6, 14195 Berlin, Germany
[8] Current address: Department of Applied Science and Technology (DISAT), Politecnico di Torino, Corso Duca degli Abruzzi 24, 10129, Turin, Italy
[9] Current address: Department of Chemistry and Biochemistry, University of Oregon, Eugene, Oregon 97403, USA

[#]These authors contributed equally
[*]Email: m.koper@chem.leidenuniv.nl, r.v.mom@lic.leidenuniv.nl, nlopez@iciq.es, imccrum@clarkson.edu, kasgun@dtu.dk, arthur.shih@northwestern.edu

Table of Contents

1. Experimentation

1.1 Cleaning

Electrochemical cells and all parts that contact the electrolyte (e.g. stirbars[1], rotation disk sheaths, etc.) should be thoroughly cleaned prior to use, to remove different contaminants affecting the electrochemical signal. The following rigorous cleaning procedure has provided reliable data and reproducible results. First, the electrochemical cell is soaked in a 0.5 M H_2SO_4 solution with 1 g L^{-1} $KMnO_4$ to oxidize organic contaminants to MnO_x deposits [2,3] for at least 24 hours at room temperature. These MnO_x deposits are then dissolved in piranha solution (~1 M H_2SO_4 and ~6% H_2O_2) for > 30 minutes at room temperature. The cell is then rinsed three times in ultrapure water and boiled at least five times, refreshing the water between boiling steps[4].

1.2 Working electrode

Since there are different opinions in the community about the best method for polishing electrodes, we will give advice based on our own experiences, a critical look at the current literature, and information provided by suppliers. A standard procedure involves sequential mechanical polishing with particle suspensions of decreasing sizes, and between different particle sizes rinsing and ultrasonicating the electrode in ultrapure water or organic solvents such as acetone and ethanol. Despite efforts in cleaning the electrode between steps or after polishing, particle residues often remain on the electrode surface [5,6]. In the case of diamond and silica particles, these are mostly chemically inert and do not influence the electrocatalytic reactions being studied. On the other hand, the presence of alumina particles on the electrode surface may strongly alter the electrochemical signal [7]. Al^{3+} lowers the barrier for water dissociation, promoting the water reduction reaction, and can undergo hydrolysis at pH ≥ 5 discharging protons at the interface [8]. For water oxidation, cations have also been shown to affect the reaction rate, even though specifically the effect of Al^{3+} has not yet been studied [9]. Considering that suppliers normally recommend alumina pastes and suspensions for polishing (precious) metals, graphite, glassy carbon and other commonly used substrates in electrocatalysis, diamond and silica are safer polishing media even though these might lead to a worse finish for soft metals. Diamond suspensions can be found nowadays with particle sizes down to 0.05 µm, which often provides an acceptable surface finish. Specifically in the case of commercial single crystalline samples, which are received polished, contaminating (polishing or carbon) particles at the surface can pin step edges and hinder the formation or large terraces upon annealing. In general, the most effective ways of removing these contaminating particles are sputtering in ultra-high vacuum, or chemically etching the surface. The chemical etching can be done, for example, using aqua regia, piranha solution, or by applying an oxidative/reductive potential in acid or base, depending on the electrode material. We note that, for soft substrates such as gold, prolonged chemical etching can generate pits on the surface [10].

During electrodeposition, the porosity is often strongly affected by the deposition protocol. Taking care of the electrochemical accessibility and mass transport in working electrodes is also a key factor for obtaining reproducible results. Several methods (use of single crystals, PVD, pulsed laser deposition, molecular beam epitaxy, ALD, grafting of molecules on single crystals etc.) have the advantage that they do offer good control over the morphology, yet are not scalable to industrial proportions.

These creative endeavors often add additional complexity and in the spirit of reproducibility, we encourage the reporting of details, no matter how small and possibly even photos/videos, to be included in the supplementary information [11,12]. For instance, active metallic impurities on seemingly metal-free carbon electrodes were also found to contribute to catalytic performance [13–15], illustrating that even impurities below the detection level of characterization instruments can hinder reproducibility.

1.3 Electrolyte

Supplying ultra-high purity solvents is imperative for reproducible studies. In aqueous electrolytes, the purity of water can be monitored by the conductance which should be ~18.2 MΩ-cm. When experiments are performed with deuterated water (D_2O)[16], we recommend purifying D_2O as it often contains metal ions and anion impurities from corrosion and radiation processes during D_2O production[17]. One way to purify D_2O is digestion with an oxidizing agent (e.g. alkaline permanganate), followed by distillation[17]. This process must be performed in a well-controlled system to minimize contamination from the atmosphere.

The presence of buffering species (e.g. phosphate, bicarbonate) in the electrolyte of choice should be carefully considered. Since buffers minimize pH variations, they affect the concentration gradients in H^+ and/or OH^- generated during electrochemical reactions. Buffer species can be rightly regarded as proton donor shuttles in acidic media and oxygen donor shuttles in alkaline media, thus affecting the electroactivity of cathodic and anodic processes, respectively [18–20]. The suppression of concentration overpotentials obtained by supporting buffer ions can be compared, even if to a different extent, to the one obtained by increasing mass transport to the surface. Reasonably, in acidic media, sustaining the concentration gradient in H^+ the buffer leads to an increase in HER activity. On the other hand, buffering species have been reported to also increase HER in neutral and alkaline conditions where water is the reactant. Under these experimental conditions (e.g., HCO_3^-/CO_3^{2-} buffer at pH ca. 10), protolysis of the buffer proton-containing species fails to explain the improved HER activity [21,22]. Alternatively, it has been proposed that the buffer proton-containing ion itself, such as HCO_3^- and $H_2PO_4^-$, may directly discharge into the surface to release a proton and should hence be considered as the reactant species for HER [21,23].

1.4 The dilution equation: revealing limitations of a pH meter

H_2SO_4 molarities were measured using two different methods: dilution equation (Supplementary Equations 1 and 2) and pH meter (Supplementary Equation 3). We observed parity between all molarities measured except at 0.5 M H_2SO_4 (pH 0.3) likely because this pH is outside of the pH meter's accuracy range. If the pH from the pH meter had been taken at face value without validation, we would have under-reported the actual concentration. Thus, we highly recommend pH meters (and other measurement devices such as weigh balances, potentiostats, etc.) to be validated by at least one or more external checks.

Dilution Equation:

$$C_1V_1 = C_2(V_1 + V_2) \qquad \text{(Supplementary Equation 1)}$$

$$C_2 = \frac{C_1V_1}{V_1+V_2} \qquad \text{(Supplementary Equation 2)}$$

Where C_1 and V_1 are the concentration and volume of the undiluted H_2SO_4 solution needing to be diluted, V_2 is the volume of water added. C_2 is the final diluted concentration.

pH Calibration Equation:

$$pH = mU + b \quad \text{(Supplementary Equation 3)}$$

Where m and b are the slope and y-intercept of the pH probe calibration, U is the potential difference (typically in mV) measured by the pH probe.

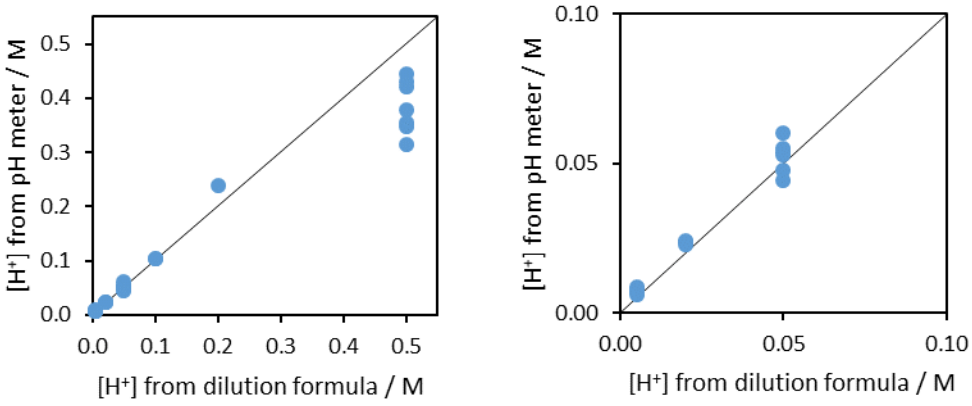

Supplementary Figure 1. Left: Parity plot for the molarity measured from the pH meter and dilution formula for H_2SO_4 between molarities of 0.005 and 0.5 M. The deviation observed at 0.5 M H_2SO_4 is because 0.5 M (pH 0.3) is outside the calibration range of the pH meter (pH 2 to 7). **Right:** Zoom-in of the parity plot to molarities less than 0.1 M. Each data point represents a newly prepared solution.

1.5 Bubble fouling

It is important to consider difference between HER and OER catalysts. Whereas HER catalysts for more fundamental studies are often relatively flat surfaces, OER catalysts are almost exclusively layered materials. These OER catalysts are often amorphous, leaving opportunities for nano/micro bubbles to get stuck [24]. For OER, it seems that the influence of bubbles is significant even at relatively low current densities [25]. Although removing all nano/micro/macro-sized gas bubbles during water electrolysis is challenging even under the convective flow , one practical approach is to minimize the effect of macro-sized gas bubbles. For instance, HER kinetic currents - obtained under low current densities where macro-sized gas bubbles are not observed - are independent of the rotation rate [26–30].

To obtain accurate kinetic parameters, gas bubble effects must be carefully excluded or corrected. A simple empirical proportional relationship between the gas bubble coverage and the rate of gas evolution reaction has been proposed [31]. However, the relation between gas bubble coverage and the effective surface area is not well understood. One approach to quantify the effective surface area is to introduce the averaged fraction of available active sites during water electrolysis; the characteristic time without gas bubble blocking can be obtained by the inverse of gas bubble

detachment frequency experimentally collected through the electrochemical noise analysis using SECM [32].

1.6 Impurities in chemicals used to clean cells, make electrolyte and purge Electrolyte

Supplementary Table 1. Purity and impurities listed by vendor for liquids used to wash glassware

Chemical **Vendor and Item ID**	**Impurities listed by manufacturer**
Ultra High Purity Water Millipore	< 5 ppb total organic content (TOC) 18.2 MΩ·cm at 25 °C
Potassium permanganate ($KMnO_4$) ≥ 99.0 % Sigma Aldrich 223468-500G	Chloride, Chlorate (as Cl^-): ≤ 0.005 % Sulfate (SO_4^{2-}): ≤ 0.02 %
Sulfuric Acid (H_2SO_4) 95.0 – 97.0 % Sigma Aldrich 30743-1L-M	Chloride (Cl^-): ≤ 0.1 mg/kg (ppm) Nitrate (NO_3^-): ≤ 0.2 mg/kg (ppm) Phosphate (PO_4^{3-}): ≤ 0.00005% (0.5 ppm)
Hydrogen Peroxide (H_2O_2) 35% Merck KGaA 108600	Sulfuric Acid (H_2SO_4): ≤ 0.025 % Pb heavy metal: ≤ 0.0002 % Chloride (Cl^-): ≤ 0.005 % Residual solvents (ICH Q3C): excluded from production process Non volatile matter: ≤ 0.10 % Residue on ignition: ≤ 0.05 % Preservatives: $Na_2H_2P_2O_7$: 0.015% H_3PO_4: 0.01% NH_4NO_3: 0.006% Sn: 0.001%

Supplementary Table 2. Purity and impurities listed by vendor for liquids for electrolyte

Chemical **Vendor and Item ID**	**Impurities listed by manufacturer**
Ultra High Purity Water Millipore	< 5 ppb total organic content (TOC) 18.2 MΩ·cm at 25 °C
Sulfuric Acid (H_2SO_4) ≥ 95 % Sigma Aldrich 77329-250ML-F	Chloride (Cl^-): ≤ 0.5 mg/kg (ppm) Nitrate (NO_3^-): ≤ 0.1 mg/kg (ppm) Phosphate (PO_4^{3-}): ≤ 0.5 mg/kg (ppm)

Supplementary Table 3. Purity listed on cylinder and impurities by vendor for gases used to purge electrolyte. No differences in the CVs and HER currents were observed between these two purities.

Chemical **Vendor and Item ID**	**Impurities listed by manufacturer**
Argon Linde 6.0 Scientific Grade ≥ 99.9999%	N_2 ≤ 0.5 ppm H_2 ≤ 0.2 ppm O_2 ≤ 0.5 ppm Total hydrocarbon content (THC) ≤ 0.1 ppm H_2O ≤ 0.5 ppm CO_2 ≤ 0.1 ppm CO ≤ 0.1 ppm
Argon Linde 5.0 grade ≥ 99.999%	N_2 ≤ 5 ppm O_2 ≤ 2 ppm Total hydrocarbon content (THC) ≤ 0.2 ppm H_2O ≤ 3 ppm
Hydrogen Linde 6.0 High Purity ≥ 99.9999%	N_2 ≤ 1 ppm O_2 ≤ 0.7 ppm Total hydrocarbon content (THC) ≤ 0.1 ppm H_2O ≤ 1 ppm CO ≤ 0.1 ppm CO_2 ≤ 0.1 ppm
Hydrogen Linde 5.0 Detector Grade ≥ 99.999%	N_2 ≤ 3 ppm Total hydrocarbon content (THC) ≤ 0.5 ppm O_2 ≤ 2 ppm H_2O ≤ 5 ppm

1.7 Overpotential window where kinetics are dominated by HER

Intrinsic Tafel behavior reflects irreversible kinetics, which only occurs at high overpotentials for reversible reactions, such as HER (Supplementary Equation 4) [33]. The total steady state current density due to a reversible chemical reaction is expressed as the sum of an oxidative and reductive current (Supplementary Equation 5). Since both oxidative and reductive currents obey a Tafel expression, the ratio of their rates can be used to calculate the overpotential window where kinetics are dominated by reduction (Supplementary Equation 6). Assuming that reduction dominates when the ratio of the oxidation and reduction currents is less than 0.01, we calculate that HER dominates at overpotentials lower than -0.06 V_{RHE} (Supplementary Equation 7).

$$2H^+ + 2e^- \underset{oxidation}{\overset{reduction}{\rightleftharpoons}} H_2 \qquad \text{(Supplementary Equation 4)}$$

$$i_{total} = i_{oxidation} + i_{reduction} \qquad \text{(Supplementary Equation 5)}$$

$$\frac{i_{reduction}}{i_{oxidation}} = \frac{i_{HER}}{i_{HOR}} = e^{\frac{2F\eta}{RT}} \qquad \text{(Supplementary Equation 6)}$$

$$\frac{i_{HOR}}{i_{HER}} = e^{\frac{2F\eta}{RT}} < 0.01 \; when \; \eta < -0.06 \; V_{RHE} \qquad \text{(Supplementary Equation 7)}$$

2. Characterization methods

Supplementary Table 4. Overview of important complementary characterization techniques for a) bulk electrodes, b) the electrode-electrolyte interface and c) reaction products in electrocatalysis.

a) Electrode *in situ* and/or *ex situ* characterization (bulk)

Technique	*Information*	*Special requirements*	*Challenges*
Raman spectroscopy [34–37]	Electrode structure (based on vibrations)	Thin electrolyte or electrode	• Bubble formation • Signal can be weak
X-ray absorption spectroscopy [38,39]	Element-resolved: • Oxidation state • Local bonding environment	Thin electrolyte or electrode	• Vacuum interface when using soft X-rays • Beam damage
X-ray diffraction [40,41]	Crystal structure	Crystalline electrode	Beam damage
Electrochemical quartz crystal microbalance [42–44]	• Ion content in pores • Electrode mass	Electrode film deposited on quartz crystal	• Interference of surface roughness and local viscosity • Bubble formation
Electron microscopy [45–48]	Electrode morphology	Ultrathin electrode (TEM) or electrode film on window (SEM)	• Beam damage • Vacuum interface • Bubble formation • Usually *ex situ*
X-ray fluorescence	Elemental composition	–	Used *ex situ*

b) Electrode-electrolyte interface *in situ* and/or *ex situ* characterization

Technique	*Information*	*Special requirements*	*Challenges*
Voltammetry techniques (cyclic voltammetry, chronoamperometry, impedance spectroscopy, etc)	Identification of oxidation/reduction events, catalytic activity, interface dynamics	Conductive substrate	No direct insight into the structure of the interface
Raman spectroscopy (plasmonically enhanced) [49–52]	Adsorbates, interfacial electrolyte structure	• Thin electrolyte • Electrode needs to be plasmonic (e.g. Au, Ag, Cu), or is coated with plasmonic particles	• Bubble formation • Preparation of plasmonic particles

Infrared spectroscopy [53–55]	Adsorbates, interfacial electrolyte structure	Thin electrolyte or electrode	• Bubble formation • IR absorption of water
X-ray absorption spectroscopy [38,39,56,57]	Element-resolved surface oxidation state, bonding environment	• Thin electrolyte or electrode • High surface-to-bulk ratio electrode	• Beam damage • Vacuum interface when using soft X-rays • Extraction of interface signal vs. bulk
X-ray photoelectron spectroscopy [39,58–61]	Element-resolved interface composition, surface oxidation state, bonding environment	Ultrathin (few nm) electrolyte or electrode	• Beam damage • Vacuum interface • Often *ex situ*
Grazing incidence X-ray scattering (SXRD/GISAXS) [62–65]	Surface structure/morphology	• Single crystal or nanoparticles on single crystal • Thin electrolyte preferred	• Beam damage • Bubble formation
Scanning probe microscopy (STM/AFM) [66–70]	Surface structure	• Single crystal electrode • Mechanically rigid cell	• Vibrations • Interference of faradaic current (STM) • Bubble formation
Scanning electrochemical probe microscopy (SECM, SICM, SIET) [71,72]	Local pH and local concentration of reactants and products, local electrochemical reactivity	• Small electrolyte volume • Selective probe	• Bubble formation • Vibrations • Electronic noise
Confocal laser scanning fluorescence microscopy (CLSFM) [73,74]	Local pH and local concentration of reactants and products	Presence of a fluorophore in the electrolyte	• Bubble formation • Interference of the fluorophore
Rotating ring disc electrode (RRDE) [75–77]	Local pH	RRDE electrode geometry, pH sensitive ring electrode	Bubble accumulation

c) Product analysis

Technique	*Information*	*Special requirements*	*Challenges*

Rotating ring disc electrode (RRDE) [75]	Quantification of one of the products	RRDE electrode geometry, selective ring electrode material	Selectivity to specific product
Gas chromatography [78,79]	Gaseous product identification	None	Time resolution
Liquid chromatography [80]	Liquid product identification	None	Time resolution
Differential electrochemical mass spectrometry [81–85]	Gaseous product identification (fast)	Low electrolyte volume preferred	• Sensitivity • Quantification • Local depletion of reactants/products
Inductively coupled plasma mass spectrometry [84,86–88]	Quantification of dissolved metals	Low electrolyte volume preferred	Interferences (mainly for 3d metals)

3. Theory considerations

The first applications of density functional theory (DFT) modeling to water electrolysis focused on defining thermodynamic descriptors for the activity of the hydrogen evolution (HER) and oxygen evolution (OER) reactions. With reference to the HER reaction, "volcano" relationship between measured HER current densities in acidic media and hydrogen binding energy (ΔG_{*H}) for different metal surfaces was reported [89]. Such "volcano" relationship between HER activities and the metal work function was previously observed experimentally [90]. Still, the introduction of the unique descriptor ΔG_{*H} was crucial to allow fast computational screening of potential HER catalysts, thus leading to enormous advances in the field [91]. The rationale behind this HER activity vs ΔG_{*H} correlation lies within the Sabatier principle [92]. An ideal catalyst for HER should bind H strong enough to enable its adsorption (Volmer step), yet weak enough to allow H_2 evolution (Heyrovský or Tafel step) [93]. However, recent investigations have highlighted that the ΔG_{*H} descriptor might be exceedingly simple, since additional materials predicted theoretically show worse performance than Pt, the current catalyst of choice [94,95]. Hence, optimal catalysts for HER should exhibit slightly endothermic ΔG_{*H} due to H coverage effects [96], and the existence of kinetic barriers also hints to optimal values of ΔG_{*H} more positive than 0 [97].

Successive studies have typically carried out an analogous "search for descriptors" protocol, including the effect of applied electrode potential through the Computational Hydrogen Electrode (CHE) scheme [98]. The CHE enables to account for the applied electrode potential in electrocatalytic steps which involve a concerted proton-coupled electron transfer (PCET) [98]. Alternative approaches are possible [99], for instance, using metal cations and OH radical as references [100,101], however the CHE stands out for the convenient choice of H_2 as reference. In fact, at 0 V vs SHE and standard conditions the chemical potential of a proton/electron transfer is equivalent to one half of the hydrogen gas one. Thus, at different potential U_{SHE} and bulk pH, the Gibbs free energy of a reaction step shifts by a factor that linearly depends on U_{SHE}, pH, and overall number (n) of PCET until that step (Supplementary Equation 8). Since the CHE framework is applicable only to PCET steps, the potential dependence is in practice versus the RHE scale, *i.e.* variations of bulk pH or potential versus SHE have an analogous effect on reaction thermodynamics. In Supplementary Equation 8, k_B is the Boltzmann constant, and T the applied temperature. The ($\pm n$) term is positive (+) for a cathodic reaction and negative (–) for an anodic reaction. By applying the CHE scheme, the theoretical limiting potential (U_L) for a given reaction can be estimated as the minimum applied potential required to make any reaction step exergonic [91]. Thus, theoretical overpotential ($\eta_{theo} = U_L - U_{eq}$), can be calculated and this parameter has been recurrently employed to predict OER and HER performance, [91,102] through corresponding "volcano" plots[102].

$$\Delta G(U_{SHE}, pH) = \pm n|e^-|(U_{SHE} + k_B\, T\, Ln(10)\, pH) \qquad \text{(Supplementary Equation 8)}$$

With reference to the OER reaction [102–106], two mechanisms have been put forward [107]. The high pH dominant di-oxygen atom recombination (I2M) requires two adsorption sites [107]. Instead, only 1 adsorption site is involved in the Water Nucleophilic Attack (WNA) scheme, which is the most common one. The WNA accounts for three intermediates, OH*, O*, and OOH* [108]. Due to the existence of thermodynamic linear scaling relationships (LSR) [109], mediated on transition metals by their *d*-band center [110] and the bond order between catalyst and adsorbate [111], ΔG_{OH*} and ΔG_{OOH*} correlate with ΔG_{O*} for metals [103] and conductive oxides [112] (ΔG = Gibbs Free energy of formation). Thus, $\Delta G_{O*} - \Delta G_{OH*}$ is typically assumed as the general descriptor for OER activity [91,102], since ΔG_{OH*}

and ΔG_{OOH*} are linearly dependent due to their equivalent adsorbate/surface bond order. These LSR dependencies between OER intermediates determine intrinsic limitations to activity as the specific reaction steps cannot be optimized separately [109], which may be overcome by introducing different binding sites [105] or tuning of local morphology [113], for instance.

While the framework based on thermodynamic descriptors and the CHE has proved effective for predicting OER and HER activity in acidic media, it showed limitations in modeling HER in alkaline media, where H_2O is expected to be the main proton source [93]. Reaction rates are in this case significantly lower than in acidic media [93], and oxophilic dopants and cations promote the kinetics of the overall reaction [8,114,115]. To tackle these novel observations, simulations have been improved toward more realistic models of the electrical double layer (EDL), which explicitly accounts for H_2O as proton donor, cations, electric field [116]. By assessing water reduction in presence of a partially solvated Na^+ cation, a "volcano" relationship between HER rates measured on decorated Pt(533) vs *OH binding strength was demonstrated [114]. Water dissociation is the rate-determining step for decorations that account for weak *OH binding (i.e. Ag), while too strong *OH binding prevents OH desorption on Mo and Re dopants. Thus, a 3D "volcano" relationship between HER rates in alkaline media and both *H and *OH binding strengths was defined[114]. In addition to the *OH activity descriptor, a mechanism for water dissociation in presence of cation (M^+) was suggested, Supplementary Equation 9, since HER on Au shows a positive reaction order on cation concentration in mildly alkaline media [115].

$$H_2O + e^- \rightarrow *H–OH^{\delta-}\cdots M^+ + (1 - \delta-)\, e^- \rightarrow *H + OH^- + M^+ \qquad \text{(Supplementary Equation 9)}$$

This cation-promoted mechanism was later confirmed through both *ab initio* molecular dynamics and static DFT simulations in presence of partially solvated multivalent cations [8]. Specifically, charged cations draw the electronic density of atomic oxygen in neighboring water toward the metal center, weakening the hydrogen bond and facilitating water dissociation. This effect depends on the electrostatic field generated by the cation, thus it is correctly described by cation acidity. In fact, the activation energy for water dissociation correlates with cation acidity, ranging from > 1.5 eV (Cs^+) to almost 0 eV for acidic cations (Al^{3+}). Besides, cation acidity also influences the cation concentration at the Outer Helmholtz Plane (OHP), since acidic cations show higher ion-ion repulsion and are less prone to accumulation. The interplay between promotion of water dissociation and accumulation at the OHP leads to a "volcano" relationship of HER activity vs cation acidity[8], where Nd^{3+} exhibits the best trade-off between both factors. On top of OH binding strength and cation acidity, the local solvation geometry close to the catalyst is another relevant parameter for HER activity in alkaline media. *Ab initio* molecular dynamics simulations are crucial for such investigations [116], as proved in a recent work [117]. In that study, the first solvation layer on Pt-coated Au(111) was defined as a network of solvated cations and H-bonded water molecules, very reactive toward dissociation.

In addition to the activity, an essential criterion for a catalytic material is its stability under harsh oxidizing and corrosive conditions. Pourbaix diagrams are an invaluable tool for exploring the corrosion profiles of materials. Aqueous stability of a catalytic material can be determined by computing the material's Gibbs free energy of formation (ΔG_{pbx}) with respect to the stable domains in the computational Pourbaix diagram [118] as a function of pH and electric potential. This approach is recently used to evaluate the aqueous stability of oxide materials[119–121]. Moreover, the ability to synthesize a promising candidate material is important and can be estimated by thermodynamic phase stability - defined as the energy of decomposition of a material into the set of most stable

materials at this chemical composition. The higher the energy of decomposition of a material, the more unstable the material is, and the more challenging the synthesis will be. Using these two descriptors, a few promising acid-stable and active oxide OER catalytic materials in the Materials Project database were identified [106].

4. References

1. Pentsak, E. O., Eremin, D. B., Gordeev, E. G. & Ananikov, V. P. Phantom Reactivity in Organic and Catalytic Reactions as a Consequence of Microscale Destruction and Contamination - Trapping Effects of Magnetic Stir Bars. *ACS Catal.* **9**, 3070–3081 (2019).

2. Fatiadi, A. J. The classical permanganate ion: Still a novel oxidant in organic chemistry. *Synthesis (Stuttg).* **1987**, 85–127 (1987).

3. Shaabani, A., Tavasoli-Rad, F. & Lee, D. G. Potassium permanganate oxidation of organic compounds. *Synth. Commun.* **35**, 571–580 (2005).

4. Arulmozhi, N., Esau, D., van Drunen, J. & Jerkiewicz, G. Design and Development of Instrumentations for the Preparation of Platinum Single Crystals for Electrochemistry and Electrocatalysis Research Part 3 : Final Treatment , Electrochemical Measurements , and Recommended Laboratory Practices. *Electrocatalysis* **9**, 113–123 (2018).

5. Kazee, B., Weisshaar, D. E. & Kuwana, T. Evidence for the Presence of a Thin Carbon-Particle Layer on Polished Glassy Carbon Electrodes. *Anal. Chem.* **57**, 2736–2739 (1985).

6. Kiema, G. K., Aktay, M. & Mcdermott, M. T. Preparation of reproducible glassy carbon electrodes by removal of polishing impurities. *J. Electroanal. Chem.* **540**, 7–15 (2003).

7. Monteiro, M. C. O. & Koper, M. T. M. Alumina contamination through polishing and its effect on hydrogen evolution on gold electrodes. *Electrochim. Acta* **325**, 134915 (2019).

8. Monteiro, M. C. O., Dattila, F., Lopez, N. & Koper, M. T. M. The Role of Cation Acidity on the Competition between Hydrogen Evolution and CO2 Reduction on Gold Electrodes. *J. Am. Chem. Soc.* **144**, 1589–1602 (2022).

9. Garcia, A. C., Touzalin, T., Nieuwland, C., Perini, N. & Koper, M. T. M. Enhancement of Oxygen Evolution Activity of Nickel Oxyhydroxide by Electrolyte Alkali Cations. *Angew. Chemie Int. Ed.* **58**, 12999–13003 (2019).

10. Monteiro, M. C. O. & Koper, M. T. M. Electrochimica Acta Alumina contamination through polishing and its effect on hydrogen evolution on gold electrodes. *Electrochim. Acta* **325**, 134915 (2019).

11. Getting to grips with Supplementary Information. *Nat. Cell Biol.* **14**, 223 (2012).

12. Pop, M. & Salzberg, S. L. Use and mis-use of supplementary material in science publications. *BMC Bioinformatics* **16**, 237 (2015).

13. Lai, L. *et al.* Exploration of the active center structure of nitrogen-doped graphene-based

catalysts for oxygen reduction reaction. *Energy Environ. Sci.* **5**, 7936–7942 (2012).

14. Wang, L., Sofer, Z. & Pumera, M. Will Any Crap We Put into Graphene Increase. doi:10.1021/acsnano.9b00184

15. Wang, L., Ambrosi, A. & Pumera, M. "Metal-Free" Catalytic Oxygen Reduction Reaction on Heteroatom-Doped Graphene is Caused by Trace Metal Impurities. *Angew. Chemie* **125**, 14063–14066 (2013).

16. Rebollar, L., Intikhab, S., Snyder, J. D. & Tang, M. H. Kinetic Isotope Effects Quantify pH-Sensitive Water Dynamics at the Pt Electrode Interface. *J. Phys. Chem. L* **11**, 2308–2313 (2020).

17. Anderson, C. E. & Ebenhaek, D. G. Heavy Water. in *Analysis of Essential Nuclear Reactor Materials* (ed. Rodden, C. J.) (U.S. Atomic Energy Commission, 1964).

18. Auinger, M. *et al.* Near-surface ion distribution and buffer effects during electrochemical reactions. *Near-surface ion Distrib. buffer Eff. Dur. Electrochem. React.* **13**, 16384–16394 (2011).

19. Marcandalli, G., Monteiro, M. C. O. & Koper, M. T. M. Electrolyte buffering species as oxygen donor shuttles in CO electrooxidation. *Phys. Chem. Chem. Phys.* **24**, 2022–2031 (2022).

20. Jung, O., Jackson, M. N., Bisbey, R. P., Kogan, N. E. & Surendranath, Y. Innocent buffers reveal the intrinsic pH- and coverage-dependent kinetics of the hydrogen evolution reaction on noble metals. *Joule* **6**, 476–493 (2022).

21. Marcandalli, G., Boterman, K. & Koper, M. T. M. Understanding hydrogen evolution reaction in bicarbonate buffer. *J. Catal.* **405**, 346–354 (2022).

22. Shinagawa, T., Obata, K. & Takanabe, K. Switching of Kinetically Relevant Reactants for the Aqueous Cathodic Process Determined by Mass-transport Coupled with Protolysis. *ChemCatChem* **11**, 5961–5968 (2019).

23. Jackson, M. N., Jung, O., Lamotte, H. C. & Surendranath, Y. Donor-Dependent Promotion of Interfacial Proton-Coupled Electron Transfer in Aqueous Electrocatalysis. *ACS Catal.* **9**, 3737–3743 (2019).

24. El-Sayed, H. A., Weiß, A., Olbrich, L. F., Putro, G. P. & Gasteiger, H. A. OER Catalyst Stability Investigation Using RDE Technique: A Stability Measure or an Artifact? *J. Electrochem. Soc.* **166**, F458–F464 (2019).

25. Barati, G., Aliofkhazraei, M. & Shanmugam, S. Recent advances in methods and technologies for enhancing bubble detachment during electrochemical water splitting. *Renew. Sustain. Energy Rev.* **114**, 109300 (2019).

26. Sheng, W., Gasteiger, H. A. & Shao-Horn, Y. Hydrogen Oxidation and Evolution Reaction Kinetics on Platinum: Acid vs Alkaline Electrolytes. *J. Electrochem. Soc.* **11**, B1529–B1536 (2010).

27. Shih, A. J., Arulmozhi, N. & Koper, M. T. M. Electrocatalysis under Cover: Enhanced Hydrogen Evolution via Defective Graphene-Covered Pt(111). *ACS Catal.* **11**, 10892–10901 (2021).

28. Williams, K., Limaye, A., Weiss, T., Chung, M. & Manthiram, K. Accounting for species' thermodynamic activities changes mechanistic interpretations of electrochemical kinetic data. *chemrxiv* (2022). doi:10.26434/chemrxiv-2022-vk5z9

29. Kita, H., Ye, S. & Gao, Y. Mass transfer effect in hydrogen evolution reaction on Pt single-crystal electrodes in acid solution. *J. Electroanal. Chem.* **334**, 351–357 (1992).

30. Gómez, R., Fernández-Vega, A., Feliu, J. M. & Aldaz, A. Hydrogen evolution on platinum single crystal surfaces: effects of irreversibly adsorbed bismuth and antimony on hydrogen adsorption and evolution on platinum (100). *J. Phys. Chem.* **97**, 4769–4776 (1993).

31. Vogt, H. & Balzer, R. J. The bubble coverage of gas-evolving electrodes in stagnant electrolytes. *Electrochim. Acta* **50**, 2073–2079 (2005).

32. Zeradjanin, A. R. Frequent Pitfalls in the Characterization of Electrodes Designed for Electrochemical Energy Conversion and Storage. *ChemSusChem* **11**, 1278–1284 (2018).

33. Zheng, J., Yan, Y. & Xu, B. Correcting the Hydrogen Diffusion Limitation in Rotating Disk Electrode Measurements of Hydrogen Evolution Reaction Kinetics. *J. Electrochem. Soc.* **162**, F1470–F1481 (2015).

34. Rabe, M. *et al.* Alkaline manganese electrochemistry studied by in situ and operando spectroscopic methods – metal dissolution, oxide formation and oxygen evolution. *Phys. Chem. Chem. Phys.* **21**, 10457–10469 (2019).

35. Huang, J. *et al.* In situ monitoring of the electrochemically induced phase transition of thermodynamically metastable 1T-MoS2 at nanoscale. *Nanoscale* **12**, 9246–9254 (2020).

36. Falling, L. J. *et al.* Graphene-Capped Liquid Thin Films for Electrochemical Operando X-ray Spectroscopy and Scanning Electron Microscopy. *ACS Appl. Mater. Interfaces* **12**, 37680–37692 (2020).

37. Ling, X. *et al.* Can Graphene be used as a Substrate for Raman Enhancement? *Nano Lett.* **10**, 553–561 (2010).

38. Timoshenko, J. & Roldan Cuenya, B. In Situ/ Operando Electrocatalyst Characterization by X-ray Absorption Spectroscopy. *Chem. Rev.* **121**, 882–961 (2021).

39. Velasco-Velez, J.-J. *et al.* A comparative study of electrochemical cells for in situ x-ray spectroscopies in the soft and tender x-ray range. *J. Phys. D. Appl. Phys.* **54**, 124003 (2021).

40. Liu, Y. *et al.* Transition Metal Nitrides as Promising Catalyst Supports for Tuning CO/H2 Syngas Production from Electrochemical CO2 Reduction. *Angew. Chemie Int. Ed.* **59**, 11345–11348 (2020).

41. Sasaki, K., Marinkovic, N., Isaacs, H. S. & Adzic, R. R. Synchrotron-Based In Situ Characterization of Carbon-Supported Platinum and Platinum Monolayer Electrocatalysts.

ACS Catal. **6**, 69–76 (2016).

42. Sugawara, Y., Yadav, A. P., Nishikata, A. & Tsuru, T. Electrochemical quartz crystal microbalance study on dissolution of platinum in acid solutions. *Electrochemistry* **75**, 359–365 (2007).

43. Levi, M. D., Salitra, G., Levy, N., Aurbach, D. & Maier, J. Application of a quartz-crystal microbalance to measure ionic fluxes in microporous carbons for energy storage. *Nat. Mater.* **8**, 872–875 (2009).

44. Shpigel, N., Levi, M. D., Sigalov, S., Daikhin, L. & Aurbach, D. In Situ Real-Time Mechanical and Morphological Characterization of Electrodes for Electrochemical Energy Storage and Conversion by Electrochemical Quartz Crystal Microbalance with Dissipation Monitoring. *Acc. Chem. Res.* **51**, 69–79 (2018).

45. Hrnjic, A. *et al.* Observing, tracking and analysing electrochemically induced atomic-scale structural changes of an individual Pt-Co nanoparticle as a fuel cell electrocatalyst by combining modified floating electrode and identical location electron microscopy. *Electrochim. Acta* **388**, 138512 (2021).

46. Velasco-Velez, J.-J. *et al.* Revealing the Active Phase of Copper during the Electroreduction of CO 2 in Aqueous Electrolyte by Correlating In Situ X-ray Spectroscopy and In Situ Electron Microscopy . *ACS Energy Lett.* **5**, 2106–2111 (2020).

47. Zhang, L., Shi, W. & Zhang, B. A review of electrocatalyst characterization by transmission electron microscopy. *J. Energy Chem.* **26**, 1117–1135 (2017).

48. Hodnik, N., Dehm, G. & Mayrhofer, K. J. J. Importance and Challenges of Electrochemical in Situ Liquid Cell Electron Microscopy for Energy Conversion Research. *Acc. Chem. Res.* **49**, 2015–2022 (2016).

49. Wang, Y.-H. *et al.* In situ Raman spectroscopy reveals the structure and dissociation of interfacial water. *Nature* **600**, 81–85 (2021).

50. Dong, J.-C. *et al.* In situ Raman spectroscopic evidence for oxygen reduction reaction intermediates at platinum single-crystal surfaces. *Nat. Energy* **4**, 60–67 (2019).

51. Li, J. F., Zhang, Y. J., Ding, S. Y., Panneerselvam, R. & Tian, Z. Q. Core-shell nanoparticle-enhanced raman spectroscopy. *Chem. Rev.* **117**, 5002–5069 (2017).

52. Huang, Y. F., Kooyman, P. J. & Koper, M. T. M. Intermediate stages of electrochemical oxidation of single-crystalline platinum revealed by in situ Raman spectroscopy. *Nat. Commun.* **7**, 1–7 (2016).

53. Kas, R., Ayemoba, O., Firet, N. J., Middelkoop, J. & Smith, W. A. In-Situ Infrared Spectroscopy Applied to the Study of the Electrocatalytic Reduction of CO2: Theory, Practice and Challenges. *ChemPhysChem* **20**, 2904–2925 (2019).

54. Zhu, S., Li, T., Cai, W.-B. & Shao, M. CO2 Electrochemical Reduction As Probed through Infrared Spectroscopy. *ACS Energy Lett.* **4**, 682–689 (2019).

55. Zhang, Z.-Q., Banerjee, S., Thoi, V. S. & Shoji Hall, A. Reorganization of Interfacial Water by an Amphiphilic Cationic Surfactant Promotes CO2 Reduction. *J. Phys. Chem. Lett.* **11**, 5457–5463 (2020).

56. Friebel, D. *et al.* Balance of Nanostructure and Bimetallic Interactions in Pt Model Fuel Cell Catalysts: In Situ XAS and DFT Study. *J. Am. Chem. Soc.* **134**, 9664–9671 (2012).

57. Wu, C. H. *et al.* The structure of interfacial water on gold electrodes studied by x-ray absorption spectroscopy. *Science (80-.).* **346**, 831–834 (2014).

58. Favaro, M. *et al.* An Operando Investigation of (Ni-Fe-Co-Ce)Ox System as Highly Efficient Electrocatalyst for Oxygen Evolution Reaction. *ACS Catal.* **7**, 1248–1258 (2017).

59. Favaro, M. *et al.* Unravelling the electrochemical double layer by direct probing of the solid/liquid interface. *Nat. Commun.* **7**, 1–8 (2016).

60. Mom, R. *et al.* The Oxidation of Platinum under Wet Conditions Observed by Electrochemical X-ray Photoelectron Spectroscopy. *J. Am. Chem. Soc.* **141**, 6537–6544 (2019).

61. Velasco-Velez, J. J. *et al.* Photoelectron Spectroscopy at the Graphene-Liquid Interface Reveals the Electronic Structure of an Electrodeposited Cobalt/Graphene Electrocatalyst. *Angew. Chemie Int. Ed.* **54**, 14554–14558 (2015).

62. Rao, R. R. *et al.* Operando identification of site-dependent water oxidation activity on ruthenium dioxide single-crystal surfaces. *Nat. Catal.* **3**, 516–525 (2020).

63. Reikowski, F. *et al.* Operando Surface X-ray Diffraction Studies of Structurally Defined Co3O4 and CoOOH Thin Films during Oxygen Evolution. *ACS Catal.* **9**, 3811–3821 (2019).

64. Gründer, Y. & Lucas, C. A. Surface X-ray diffraction studies of single crystal electrocatalysts. *Nano Energy* **29**, 378–393 (2016).

65. Bogar, M. *et al.* Interplay among Dealloying, Ostwald Ripening, and Coalescence in PtXNi100-XBimetallic Alloys under Fuel-Cell-Related Conditions. *ACS Catal.* **11**, 11360–11370 (2021).

66. Jacobse, L., Rost, M. J. & Koper, M. T. M. Atomic-Scale Identification of the Electrochemical Roughening of Platinum. *ACS Cent. Sci.* **5**, 1920–1928 (2019).

67. Wang, X. *et al.* In Situ Scanning Tunneling Microscopy of Cobalt-Phthalocyanine-Catalyzed CO2 Reduction Reaction. *Angew. Chemie* **59**, 16098–16103 (2020).

68. Liang, Y. *et al.* Electrochemical Scanning Probe Microscopies in Electrocatalysis. *Small Methods* **3**, 1800387 (2019).

69. Simon, G. H., Kley, C. S. & Roldan Cuenya, B. Potential-Dependent Morphology of Copper Catalysts During CO2 Electroreduction Revealed by In Situ Atomic Force Microscopy. *Angew. Chemie Int. Ed.* **60**, 2561–2568 (2021).

70. Haid, R. W., Kluge, R. M., Schmidt, T. O. & Bandarenka, A. S. In-situ detection of active sites for carbon-based bifunctional oxygen reduction and evolution catalysis. *Electrochim. Acta*

382, 138285 (2021).

71. Monteiro, M. C. O., Jacobse, L., Touzalin, T. & Koper, M. T. M. Mediator-Free SECM for Probing the Diffusion Layer pH with Functionalized Gold Ultramicroelectrodes. *Anal. Chem.* **92**, 2237–2243 (2020).

72. Monteiro, M. C. O., Jacobse, L. & Koper, M. T. M. Understanding the Voltammetry of Bulk CO Electrooxidation in Neutral Media through Combined SECM Measurements. *J. Phys. Chem. Lett.* **11**, 9708–9713 (2020).

73. Cannan, S., Macklam, I. D. & Unwin, P. R. Three-dimensional imaging of proton gradients at microelectrode surfaces using confocal laser scanning microscopy. *Electrochem. commun.* **4**, 886–892 (2002).

74. Fuladpanjeh-Hojaghan, B. *et al.* In-Operando Mapping of pH Distribution in Electrochemical Processes. *Angew. Chemie Int. Ed.* **58**, 16815–16819 (2019).

75. Vos, J. G. & Koper, M. T. M. M. Examination and prevention of ring collection failure during gas-evolving reactions on a rotating ring-disk electrode. *J. Electroanal. Chem.* **850**, 113363 (2019).

76. Yokoyama, Y. *et al.* In Situ Local pH Measurements with Hydrated Iridium Oxide Ring Electrodes in Neutral pH Aqueous Solutions. *Chem. Lett.* **49**, 195–198 (2020).

77. Monteiro, M. C. O., Liu, X., Hagedoorn, B. J. L., Snabilié, D. D. & Koper, M. T. M. Interfacial pH Measurements Using a Rotating Ring-Disc Electrode with a Voltammetric pH Sensor. *ChemElectroChem* **9**, e202101223 (2022).

78. Wang, X. *et al.* Mechanistic reaction pathways of enhanced ethylene yields during electroreduction of CO2–CO co-feeds on Cu and Cu-tandem electrocatalysts. *Nat. Nanotechnol.* **14**, 1063–1070 (2019).

79. Davies, B. J. V., Arenz, M., Rossmeisl, J. & Escudero-Escribano, M. Electrochemical Synthesis of High-Value Chemicals: Detection of Key Reaction Intermediates and Products Combining Gas Chromatography − Mass Spectrometry and in Situ Infrared Spectroscopy. *J. Phys. Chem. C* **123**, 12762–12772 (2019).

80. Kwon, Y. & Koper, M. T. M. Combining Voltammetry with HPLC: Application to Electro-Oxidation of Glycerol. *Anal. Chem.* **82**, 5420–5424 (2010).

81. Zeng, R. *et al.* Methanol Oxidation Using Ternary Ordered Intermetallic Electrocatalysts: A DEMS Study. *ACS Catal.* **10**, 770–776 (2020).

82. Stoerzinger, K. A. *et al.* Orientation-Dependent Oxygen Evolution on RuO2 without Lattice Exchange. *ACS Energy Lett.* **2**, 876–881 (2017).

83. Todoroki, N., Tsurumaki, H., Tei, H., Mochizuki, T. & Wadayama, T. Online Electrochemical Mass Spectrometry Combined with the Rotating Disk Electrode Method for Direct Observations of Potential-Dependent Molecular Behaviors in the Electrode Surface Vicinity. *J. Electrochem. Soc.* **167**, 106503 (2020).

84. Geiger, S. *et al.* The stability number as a metric for electrocatalyst stability benchmarking. *Nat. Catal.* **1**, 508–515 (2018).

85. Scott, S. B. *et al.* The low overpotential regime of acidic water oxidation part I: the importance of O2 detection. *Energy Environ. Sci.* (2022). doi:10.1039/d1ee03914h

86. Lopes, P. P. *et al.* Relationships between Atomic Level Surface Structure and Stability/Activity of Platinum Surface Atoms in Aqueous Environments. *ACS Catal.* **6**, 2536–2544 (2016).

87. Kasian, O. *et al.* Degradation of iridium oxides via oxygen evolution from the lattice: correlating atomic scale structure with reaction mechanisms. *Energy Environ. Sci.* **12**, 3548–3555 (2019).

88. Klemm, S. O., Topalov, A. A., Laska, C. A. & Mayrhofer, K. J. J. Coupling of a high throughput microelectrochemical cell with online multielemental trace analysis by ICP-MS. *Electrochem. commun.* **13**, 1533–1535 (2011).

89. Nørskov, J. K. *et al.* Trends in the Exchange Current for Hydroge Evolution. *J. Electrochem. Soc.* **152**, J23–J26 (2005).

90. Trasatti, S. Work function, electronegativity, and electrochemical behaviour of metals. III. Electrolytic hydrogen evolution in acid solutions. *J. Electroanal. Chem.* **39**, 163–184 (1972).

91. Montoya, J. H. *et al.* Materials for solar fuels and chemicals. *Nat. Mater.* **16**, 70–81 (2017).

92. Sabatier, P. La catalyse en chimie organique. *Berange, Paris* (1920).

93. Dubouis, N. & Grimaud, A. The hydrogen evolution reaction: from material to interfacial descriptors. *Chem. Sci.* **10**, 9165–9181 (2019).

94. Hansen, J. N. *et al.* Is There Anything Better than Pt for HER? *ACS Energy Lett.* **6**, 1175–1180 (2021).

95. Rebollar, L. *et al.* "Beyond Adsorption" Descriptors in Hydrogen Electrocatalysis. *ACS Catal.* **10**, 14747–14762 (2020).

96. Lindgren, P., Kastlunger, G. & Peterson, A. A. A Challenge to the G $\sim$0 Interpretation of Hydrogen Evolution. *ACS Catal.* **10**, 121–128 (2020).

97. Exner, K. S. Electrochemistry Hydrogen electrocatalysis revisited: Weak bonding of adsorbed hydrogen as the design principle for active electrode materials. *Curr. Opin. Electrochem.* **26**, 100673 (2021).

98. Nørskov, J. K. *et al.* Origin of the Overpotential for Oxygen Reduction at a Fuel-Cell Cathode. *J. Phys. Chem. B* **108**, 17886–17892 (2004).

99. Abidi, N., Lim, K. R. G., Seh, Z. W. & Steinmann, S. N. Atomistic modeling of electrocatalysis : Are we there yet ? *WIREs Comput Mol Sci.* **11**, 1–27 (2021).

100. Anderson, A. B. & Ray, N. K. Structures and reactions of hydronium, water, and hydroxyl on an iron electrode. Potential dependence. *J. Phys. Chem.* **86**, 488–494 (1982).

101. Roques, J. & Anderson, A. B. Theory for the potential shift for OHads formation on the Pt-skin on Pt3Cr(111) in acid. *J. Electrochem. Soc.* **151**, E85–E91 (2004).

102. Man, I. C. *et al.* Universality in Oxygen Evolution Electrocatalysis on Oxide Surfaces. 1159–1165 (2011). doi:10.1002/cctc.201000397

103. Rossmeisl, J., Logadottir, A. & Nørskov, J. K. Electrolysis of water on (oxidized) metal surfaces. *Chem. Phys.* **319**, 178–184 (2005).

104. Rossmeisl, J., Qu, Z.-W., Zhu, H., Kroes, G.-J. & Nørskov, J. K. Electrolysis of water on oxide surfaces. *J. Electroanal. Chem.* **607**, 83–89 (2007).

105. Halck, N. B., Petrykin, V., Krtil, P. & Rossmeisl, J. Beyond the volcano limitations in electrocatalysis-oxygen evolution reaction. *Phys. Chem. Chem. Phys.* **16**, 13682 (2014).

106. Gunasooriya, G. T. K. K. & Nørskov, J. K. Analysis of Acid-Stable and Active Oxides for the Oxygen Evolution Reaction. *ACS Energy Lett.* **5**, 3778–3787 (2020).

107. Fang, Y. H. & Liu, Z. P. Mechanism and tafel lines of electro-oxidation of water to oxygen on RuO2(110). *J. Am. Chem. Soc.* **132**, 18214–18222 (2010).

108. Montoya, J. H. *et al.* Materials for solar fuels and chemicals. *Nat. Mater.* **16**, 70–81 (2017).

109. Pérez-Ramírez, J. & López, N. Strategies to break linear scaling relationships. *Nat. Catal.* **2**, 971–976 (2019).

110. Hammer, B. & Nørskov, J. K. Electronic factors determining the reactivity of metal surfaces. *Surf. Sci.* **343**, 211–220 (1995).

111. Abild-Pedersen, F. *et al.* Scaling Properties of Adsorption Energies for Hydrogen-Containing Molecules on Transition-Metal Surfaces. *Phys. Rev. Lett.* **99**, 016105 (2007).

112. Rossmeisl, J., Qu, Z.-W., Zhu, H., Kroes, G.-J. & Norskov, J. K. Electrolysis of water on oxide surfaces. *J. Electroanal. Chem.* **607**, 83–89 (2007).

113. Calle-Vallejo, F., Martínez, J. I., García-Lastra, J. M., Sautet, P. & Loffreda, D. Fast Prediction of Adsorption Properties for Platinum Nanocatalysts with Generalized Coordination Numbers. *Angew. Chemie* **126**, 1–5 (2014).

114. McCrum, I. T. & Koper, M. T. M. The role of adsorbed hydroxide in hydrogen evolution reaction kinetics on modified platinum. *Nat. Energy* **5**, 891–899 (2020).

115. Goyal, A. & Koper, M. T. M. The Interrelated Effect of Cations and Electrolyte pH on the Hydrogen Evolution Reaction on Gold Electrodes in Alkaline Media. *Angew. Chemie Int. Ed.* **60**, 13452–13462 (2021).

116. Groß, A. & Sakong, S. Ab initio simulations of water/metal interfaces. *Chem. Rev.* **122**, 10746–10776 (2022).

117. Wang, Y.-H. *et al.* In situ Raman spectroscopy reveals the structure and dissociation of interfacial water. *Nature* **600**, 81–86 (2021).

118. Ong, S. P. *et al.* Python Materials Genomics (pymatgen): A robust, open-source python

library for materials analysis. *Comput. Mater. Sci.* **68**, 314–319 (2013).

119. Singh, A. K. *et al.* Electrochemical Stability of Metastable Materials. *Chem. Mater.* **29**, 10159–10167 (2017).

120. Zhou, L. *et al.* Rutile Alloys in the Mn−Sb−O System Stabilize Mn3+ To Enable Oxygen Evolution in Strong Acid. *ACS Catal.* **8**, 10938–10948 (2018).

121. Gunasooriya, G. T. K. K. *et al.* First-Row Transition Metal Antimonates for the Oxygen Reduction Reaction. *ACS Nano* **16**, 6334–6348 (2022).